

Energy Extraction via Magnetic Reconnection in Konoplya-Rezzolla-Zhidenko Parametrized Black Holes

Shao-Jun Zhang^{1,2,*}

¹*Institute for Theoretical Physics and Cosmology, Zhejiang*

University of Technology, Hangzhou 310032, China

²*United Center for Gravitational Wave Physics, Zhejiang University of Technology, Hangzhou 310032, China*

(Dated: April 30, 2024)

Recently, Comisso and Asenjo proposed a novel mechanism for harnessing energy from black holes through magnetic reconnection. Our study focuses on exploring the utilization of this mechanism on Konoplya-Rezzolla-Zhidenko (KRZ) parametrized black holes to assess the impact of deformation parameters on energy extraction. Among the various parameters, $\{\delta_1, \delta_2\}$ are identified as the most important factors affecting the physics under consideration. The influence of these two parameters on the ergoregion, circular geodesics in the equatorial plane, and energy extraction from the KRZ black holes through magnetic reconnection is carefully analyzed. Results indicate that deviations from the Kerr metric have a notable influence on the energy extraction process. Particularly, energy extraction is enhanced with more negative δ_1 or more positive δ_2 within the range constrained by current astronomical observations, resulting in significantly higher maximum power and efficiency compared to the Kerr model. Moreover, when δ_2 is sufficiently negative, extracting energy through this mechanism becomes increasingly challenging, necessitating an exceptionally high black hole spin.

I. INTRODUCTION

Black holes, unique and compact objects predicted by Einstein's theory of gravity, have a significant impact on contemporary physics. Recent advances in astronomical observations have ushered in a golden age for delving into the physics of black holes [1–6]. These mysterious objects are thought to be responsible for several energetic astrophysical phenomena, such as gamma-ray bursts (GRBs) and relativistic jets in active galactic nuclei (AGNs). The energy discharged during these phenomena may originate from the gravitational potential energy liberated as matter plunges into the black hole, or from the inherent energy of the black hole itself.

According to general relativity (GR), rotating black holes have significant amounts of energy

* sjzhang@zjut.edu.cn

that can be harnessed. The second law of black hole thermodynamics states that the maximum energy that can be extracted from a rotating black hole is about $0.29Mc^2$ [7], where M is the mass of the black hole and c is the speed of light in vacuum. This energy originates from the black hole's rotational energy, prompting an intriguing inquiry into the processes involved in extracting such a significant fraction of the black hole's energy.

The first plausible mechanism for energy extraction from black holes was proposed by Penrose in 1969, now known as the Penrose process [8]. The Penrose process involves the splitting of a particle in the ergoregion into two particles. Measured from infinity, one of these particles may carry negative energy, while the other carries excess positive energy. The extraction of energy from a black hole occurs when the negative energy particle is absorbed by the black hole and the positive energy particle escapes. However, the Penrose process is considered impractical because it requires the two newborn particles to have relative velocities greater than $1/2$ the speed of light, an event thought to be rare in real astrophysical processes [9, 10]. Inspired by Penrose's work, physicists have proposed several alternative mechanisms for harnessing energy from black holes, including superradiant scattering [11], the collisional Penrose process [12], the Blandford-Znajek (BZ) process [13], and the magnetohydrodynamic (MHD) Penrose process [14]. Among these mechanisms, the BZ process is currently regarded as the most promising for elucidating GRBs [15–17] and relativistic jets in AGNs [18–21].

Recently, based on an exploratory study [22], a novel mechanism for black hole energy extraction has been proposed by Comisso and Asenjo [23]. In this mechanism, energy extraction is realized by a process of magnetic reconnection in the ergoregion of a rotating black hole. The process begins with the magnetic field around the black hole forming antiparallel configurations near the equatorial plane due to the black hole's rotation [24–27]. The jumps in the magnetic field direction induce the formation of current sheets between them, which are destroyed by plasmoid instability when their aspect ratio exceeds a critical value [28–30], resulting in the formation of plasmoids/flux ropes that drive fast magnetic reconnection to convert magnetic energy into plasma kinetic energy [31, 32]. Eventually, the plasma is expelled from the reconnection layer and the tension in the magnetic field is released as the plasma flows out. The magnetic field lines are then reextended by the dragging of the black hole to form an antiparallel configuration, and the current sheet is induced again to repeat the magnetic reconnection process. During each magnetic reconnection, the plasma in the current sheet splits into two parts, one corotating with the black hole and the other counter-rotating. The corotating part is accelerated while the counter-rotating part is decelerated. Similar to the Penrose process, if the decelerated part has negative energy and is absorbed by the

black hole, while the accelerated part escapes, the accelerated part ends up carrying extra energy, thus realizing energy extraction from the black hole. This extra energy comes from the black hole's rotational energy.

Astronomical observations have confirmed that there are often different scales of magnetic fields around black holes due to the presence of accretion matter or companion stars. For example, the supermassive black hole Sagittarius A* is accompanied by the magnetar SGR J1745-2900 [33–36], and a strong magnetic field is also present near the event horizon of the black hole in M87* [37]. Therefore, the process of magnetic reconnection of black holes can be expected to occur routinely. In fact, in the BZ mechanism, energy extraction is also realized with the help of the magnetic field around the black hole. The Comisso-Asenjo mechanism is distinguished from the BZ mechanism by its bursty nature and reliance on nonzero particle inertia. Studies by Comisso and Asenjo suggest that this mechanism may be more efficient than the BZ process in certain parameter spaces, making it a promising candidate for energy extraction from black holes.

On the other hand, to test GR and the Kerr hypothesis, it is necessary to construct other non-Kerr rotating black holes. There are usually two ways to construct them, the top-down approach and the bottom-up approach. In the top-down method, one starts from a modified gravitational theory and obtains exact rotating black hole solutions by solving the gravitational field equations. However, solving modified gravitational field equations is generally very challenging due to their complexity. Only in a few cases or under certain approximations (e.g., slow rotation) can exact analytical or numerical rotating black hole solutions be obtained, e.g., the Einstein-dilaton-Gauss-Bonnet black holes [38–42], the Chern-Simons black holes [43–46], and the Kerr-Sen black holes [47]. Conversely, the bottom-up method involves constructing parametrized black holes by generalizing the Kerr metric based on considerations like symmetries and regularity, which are independent of any specific gravity theory [48–52]. These non-Kerr rotating black holes usually contain several deformation parameters introduced to characterize the deviations from the Kerr black hole. Several of them align well with present-day astronomical observations, indicating that their presence cannot be discounted. Consequently, they may offer viable alternatives to the Kerr metric given the current level of accuracy in astronomical observations. Studies of black hole energy extraction via the Comisso-Asenjo mechanism have also been extended to these non-Kerr rotating black holes, such as spinning braneworld black holes [53], the Johannsen-Psaltis metric [54], Kerr-Sen and Kiselev black holes [55], rotating black holes with broken Lorentz symmetry [56], spinning regular black hole [57], spinning hairy black hole [58], Kerr-MOG black holes [59], Kerr-Newman-MOG black holes [60] and Kerr-de Sitter black holes [61]. These studies have demonstrated that deviations

from the Kerr black hole significantly impact the energy extraction process.

Inspired by these studies, our main goal in this paper is to study the energy extraction process via the Comisso-Asenjo mechanism for KRZ parametrized black holes [50]. The KRZ metric is proposed to describe generic stationary and axisymmetric black holes. It has several subtle advantages over other parametrized metrics. In the weak-gravity regime, it can be well-aligned with Kerr black holes and thus passes the current astronomical observational constraints, while in the near-horizon strong-gravity regime, it needs only a few dominant parameters to sufficiently describe generic deviations from the Kerr black hole. Moreover, the KRZ metric can be mapped to many top-down metrics when the deformation parameters take on some specific values. Due to these merits, it has been utilized to test GR and the Kerr hypothesis using current astronomical data, leading to the examination of constraints on the deformation parameters [62–67]. This study primarily focuses on the impact of these deformation parameters, which signify deformations near the horizon, on the magnetic reconnection process and subsequent energy extraction. Given that magnetic reconnection occurs in the near-horizon ergoregion, it is anticipated that these deformation parameters will exert notable influences on this process. Future precise astronomical observations, particularly in the strong field region near the horizon, may facilitate the testing of Kerr’s hypothesis by imposing constraints on these deformation parameters through this process.

The paper is organized as follows. In Sec. II, a brief overview of the KRZ-parametrized black hole is provided, along with an examination of how the deformation parameters impact the ergoregion. Section III delves into a thorough analysis of the circular geodesic motion of the plasma in the equatorial plane. Section IV investigates the extraction of energy from the black hole via the Comisso-Asenjo mechanism. The last section is the summary and conclusions. Throughout this work, we utilize the units $c = G = 1$, where c and G are the speed of light in vacuum and the Newton gravitational constant, respectively.

II. THE KRZ PARAMETRIZED BLACK HOLE

In Boyer-Lindquist coordinates, the KRZ metric reads [50, 62, 63],

$$ds^2 = -\frac{N^2 - W^2 \sin^2 \theta}{K^2} dt^2 - 2Wr \sin^2 \theta dt d\phi + K^2 r^2 \sin^2 \theta d\phi^2 + \frac{\Sigma B^2}{N^2} dr^2 + \Sigma r^2 d\theta^2, \quad (1)$$

where

$$N^2 = \left(1 - \frac{r_0}{r}\right) \left(1 - \frac{\epsilon_0 r_0}{r} + (k_{00} - \epsilon_0) \frac{r_0^2}{r^2} + \frac{\delta_1 r_0^3}{r^3}\right) + \left(\frac{a_{20} r_0^3}{r^3} + \frac{a_{21} r_0^4}{r^4} + \frac{k_{21} r_0^3}{r^3 \left(1 + \frac{k_{22} \left(1 - \frac{r_0}{r}\right)}{1 + k_{23} \left(1 - \frac{r_0}{r}\right)}\right)}\right) \cos^2 \theta, \quad (2)$$

$$B = 1 + \frac{\delta_4 r_0^2}{r^2} + \frac{\delta_5 r_0^2}{r^2} \cos^2 \theta, \quad (3)$$

$$W = \frac{1}{\Sigma} \left(\frac{\omega_{00} r_0^2}{r^2} + \frac{\delta_2 r_0^3}{r^3} + \frac{\delta_3 r_0^3}{r^3} \cos^2 \theta\right), \quad (4)$$

$$K^2 = 1 + \frac{aW}{r} + \frac{1}{\Sigma} \left(\frac{k_{00} r_0^2}{r^2} + \left(\frac{k_{20} r_0^2}{r^2} + \frac{k_{21} r_0^3}{r^3 \left(1 + \frac{k_{22} \left(1 - \frac{r_0}{r}\right)}{1 + k_{23} \left(1 - \frac{r_0}{r}\right)}\right)}\right) \cos^2 \theta\right), \quad (5)$$

$$\Sigma = 1 + \frac{a^2}{r^2} \cos^2 \theta, \quad (6)$$

where $a = J/M^2$ is the dimensionless spin parameter, $r_0 = 1 + \sqrt{1 - a^2}$ is the radius of the event horizon in the equatorial plane and

$$\begin{aligned} \epsilon_0 &= \frac{2 - r_0}{r_0}, & a_{20} &= \frac{2a^2}{r_0^3}, & a_{21} &= -\frac{a^4}{r_0^4} + \delta_6, & \omega_{00} &= \frac{2a}{r_0^2}, \\ k_{00} &= k_{23} = \frac{a^2}{r_0^2}, & k_{20} &= 0, & k_{21} &= \frac{a^4}{r_0^4} - \frac{2a^2}{r_0^3} - \delta_6, & k_{22} &= -\frac{a^2}{r_0^2}. \end{aligned} \quad (7)$$

Note that in the metric, the black hole mass has been set to be $M = 1$, so all physical quantities are measured in units of M in the following. Here $\{\delta_i\} (i = 1, 2, \dots, 6)$ are six deformation parameters introduced to characterize deviations away from the Kerr metric: δ_1 corresponds to deformations of g_{tt} , δ_2 and δ_3 correspond to rotational deformations of the metric, δ_4 and δ_5 correspond to deformations of g_{rr} , and δ_6 corresponds to deformations of the event horizon. In the limit of all $\delta_i \rightarrow 0$, the KRZ metric reproduces the Kerr metric exactly. Note that in the metric the sign of a can be absorbed into $\{\delta_2, \delta_3\}$ and by redefining t , so we will only consider $a > 0$. Moreover, as we see later, among the six deformation parameters, $\{\delta_1, \delta_2\}$ are the most important for the physics we are going to study. So, for simplicity we will set $\delta_3 = \delta_4 = \delta_5 = \delta_6 = 0$ in the following and only consider the influences of $\{\delta_1, \delta_2\}$. The constraint on $\{\delta_1, \delta_2\}$ from x-ray observations of the supermassive BH in Ark 564 is [63]

$$-0.27 < \delta_1 < 0.28, \quad -0.37 < \delta_2 < 0.22. \quad (8)$$

The location of the event horizon is given by the root of the equation [50]

$$N^2(r, \theta) = 0. \quad (9)$$

For nonvanishing deformation parameters, the above equation determines the radius of the event horizon as a function of the polar angle θ . The ergoregion, where magnetic reconnection occurs, lies between the event horizon and the ergosphere (the static limit surface) and is defined as

$$0 < N^2(r, \theta) < W^2 \sin^2 \theta. \quad (10)$$

In the equatorial plane $\theta = \pi/2$, the event horizon is at $r = r_0$, while the location of the ergosphere $r = r_{sl}$ is only affected by $\{\delta_1, \delta_2\}$. Figure 1 shows the ergosphere $r = r_{sl}$ in the equatorial plane as a function of $\{\delta_1, \delta_2\}$ for various values of the spin a . It can be seen that the deformation parameters $\{\delta_1, \delta_2\}$ have a significant influence on the shape of the ergoregion. From the left panel, it can be seen that a larger a results in a larger ergoregion. And for a fixed a , r_{sl} is a monotonically decreasing function of δ_1 , meaning that negative δ_1 enlarges the ergoregion while positive δ_1 shrinks it. The effect of δ_2 on r_{sl} is more complicated, as shown in the right panel. For fixed and large a , r_{sl} is a monotonically increasing function of δ_2 , meaning that positive δ_2 will expand the ergoregion, while negative δ_2 will contract it. While for fixed and small a , r_{sl} is a convex function of δ_2 , meaning that large negative δ_2 will also expand the ergoregion in this case. Note that if δ_2 is sufficiently negative, a higher (but still small) spin a is not necessary to produce a larger ergoregion (e.g., the ergoregion for $a = 0.5$ is smaller than that for $a = 0.1$ when δ_2 is large negative).

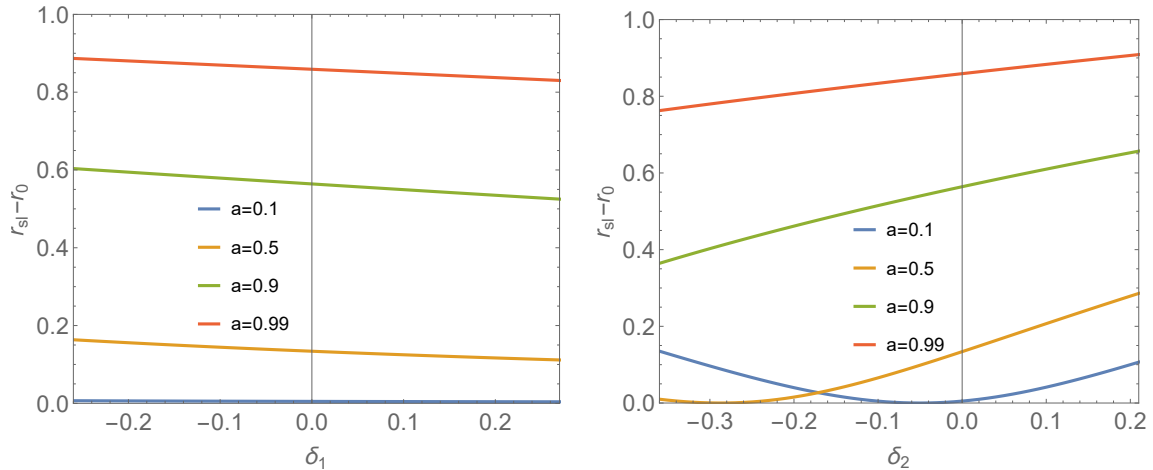


FIG. 1. Ergosphere in the equatorial plane $r = r_{sl}$ as a function of $\{\delta_1, \delta_2\}$ for various a . The event horizon in the equatorial plane is located at $r = r_0 = 1 + \sqrt{1 - a^2}$. In the left panel $\delta_2 = 0$, while in the right panel $\delta_1 = 0$.

III. CIRCULAR GEODESICS MOTION IN EQUATORIAL PLANE

Magnetic reconnection is related to the motion of charged plasma around the compact object. Under the "force-free" assumption, the electromagnetic interaction between plasma vanishes and the particles follow geodesics which can be determined by the Lagrangian

$$\mathcal{L} = \frac{1}{2}g_{\mu\nu}\dot{x}^\mu\dot{x}^\nu, \quad (11)$$

where dot means the derivative with respect to some affine parameter. From the conservation of the rest mass, $\mathcal{L} = -1/2$, we have

$$g_{rr}\dot{r}^2 + g_{\theta\theta}\dot{\theta}^2 = V_{\text{eff}}(r, \theta), \quad (12)$$

where the effective potential is

$$V_{\text{eff}}(r, \theta) = -\left(1 + g_{tt}\dot{t}^2 + 2g_{t\phi}\dot{t}\dot{\phi} + g_{\phi\phi}\dot{\phi}^2\right). \quad (13)$$

Note that L does not depend on either t or ϕ explicitly, so both the specific energy E and the z -component angular momentum L_z of the particles are conserved along geodesics,

$$E \equiv -\frac{\partial L}{\partial \dot{t}} = -g_{tt}\dot{t} - g_{t\phi}\dot{\phi}, \quad (14)$$

$$L_z \equiv \frac{\partial L}{\partial \dot{\phi}} = g_{\phi\phi}\dot{\phi} + g_{t\phi}\dot{t}. \quad (15)$$

From the above equations, we then have

$$\dot{t} = \frac{g_{\phi\phi}E + g_{t\phi}L_z}{g_{t\phi}^2 - g_{tt}g_{\phi\phi}}, \quad (16)$$

$$\dot{\phi} = -\frac{g_{t\phi}E + g_{tt}L_z}{g_{t\phi}^2 - g_{tt}g_{\phi\phi}}. \quad (17)$$

With these relations, the effective potential (13) can be rewritten as

$$V_{\text{eff}}(r, \theta) = \frac{g_{\phi\phi}E^2 + 2g_{t\phi}EL_z + g_{tt}L_z^2}{g_{t\phi}^2 - g_{tt}g_{\phi\phi}} - 1. \quad (18)$$

For circular orbits in the equatorial plane $\theta = \pi/2$, the effective potential should satisfy the following three conditions:

$$V_{\text{eff}} = 0, \quad \partial_r V_{\text{eff}} = 0, \quad \partial_\theta V_{\text{eff}} = 0. \quad (19)$$

The last condition can always be satisfied due to the reflection symmetry of the spacetime with respect to the equatorial plane. With the first two conditions, one can obtain the Keplerian

angular velocity $\Omega_K \equiv \dot{\phi}/\dot{t}$, the specific energy E and the z -component angular momentum L_z of the particle,

$$\Omega_K = \frac{-\partial_r g_{t\phi} \pm \sqrt{(\partial_r g_{t\phi})^2 - (\partial_r g_{tt})(\partial_r g_{\phi\phi})}}{\partial_r g_{\phi\phi}}, \quad (20)$$

$$E = -\frac{g_{tt} + g_{t\phi}\Omega_K}{\sqrt{-g_{tt} - 2g_{t\phi}\Omega_K - g_{\phi\phi}\Omega_K^2}}, \quad (21)$$

$$L_z = \frac{g_{t\phi} + g_{\phi\phi}\Omega_K}{\sqrt{-g_{tt} - 2g_{t\phi}\Omega_K - g_{\phi\phi}\Omega_K^2}}, \quad (22)$$

where the sign $+$ stands for corotating orbits and $-$ for counter-rotating orbits. Note that of the six deformation parameters, only $\{\delta_1, \delta_2\}$ enter the three equations above. Given the values of the spin a and the deformation parameters $\{\delta_1, \delta_2\}$, the above equations determine Ω_K, E and L_z as a function of the radius of the circular orbit. The circular orbit is stable under perturbations if $\partial_r^2 V_{\text{eff}} \leq 0$ and $\partial_\theta^2 V_{\text{eff}} \leq 0$. A radially stable circular orbit exists from infinity to the innermost (radially) stable circular orbit (ISCO), which is given by the condition

$$\partial_r^2 V_{\text{eff}} = 0. \quad (23)$$

With the above condition, the radius of ISCO can be derived for given values of the spin a and $\{\delta_1, \delta_2\}$.

In Figs. 2 and 3 we plot the radius of the ISCO as a function of the spin a for several typical values of $\{\delta_1, \delta_2\}$. The Kerr case is also shown for comparison. In each figure, we set one of the two parameters $\{\delta_1, \delta_2\}$ to zero and study the influence of the other. From the figures, we can see that as the spin a increases, the radius of the counter-rotating ISCO r_{ISCO}^- increases monotonically and is always outside the ergoregion. Therefore, we will focus only on the corotating orbits. As the spin a is increased, the radius of the corotating ISCO r_{ISCO}^+ decreases almost monotonically. The only exception is when $\delta_1 < 0$ and a is close to its extreme value $a = 1$, where r_{ISCO}^+ increases with increasing a . The corotating ISCO will enter the ergoregion when the spin a is high enough to exceed some critical value a_c . From the figures, one can see that δ_1 has little effect on a_c , while δ_2 has a significant effect on a_c . As $|\delta_2|$ is increased, a_c increases for $\delta_2 < 0$ and decreases for $\delta_2 > 0$. Since magnetic reconnection is related to orbits within the ergoregion, these results imply that for larger $|\delta_2|$, magnetic reconnection can occur for lower black hole spin if $\delta_2 > 0$, while for $\delta_2 < 0$ higher spin is required for magnetic reconnection to occur. Furthermore, r_{ISCO}^+ does not coincide with the event horizon r_0 in the extreme limit when $\delta_1 \neq 0$, and $r_{\text{ISCO}}^+ \neq r_{\text{ISCO}}^-$ in the nonrotating limit $a = 0$ if $\delta_2 \neq 0$.

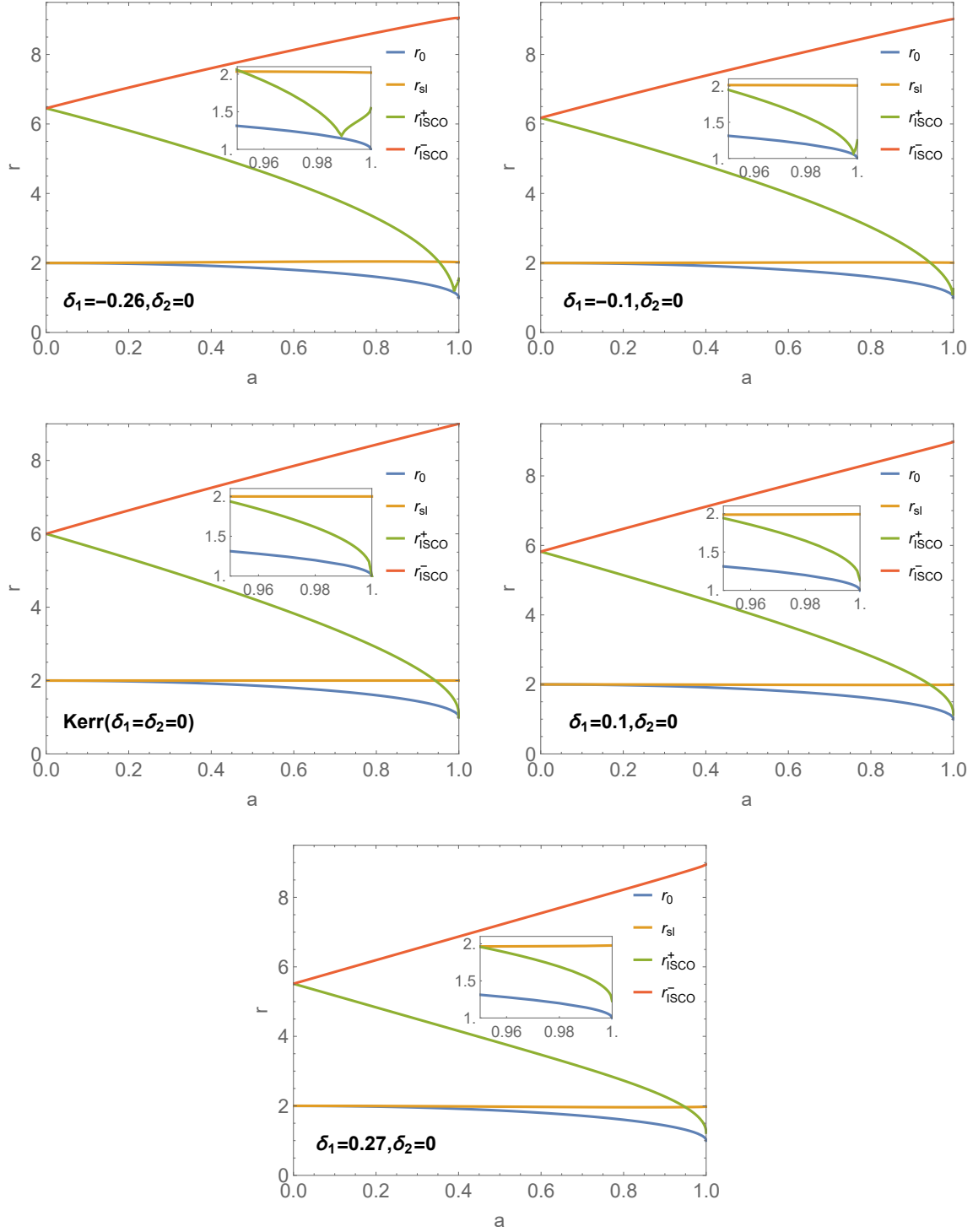


FIG. 2. Radius of innermost stable circular orbit as a function of the spin a . Here, we fix $\delta_2 = 0$ and study the influence of δ_1 . The Kerr case ($\delta_1 = \delta_2 = 0$) is also shown for comparison. r_{ISCO}^+ and r_{ISCO}^- represent the corotating and counter-rotating orbits, respectively. r_0 is the event horizon and r_{sl} is the ergosphere.

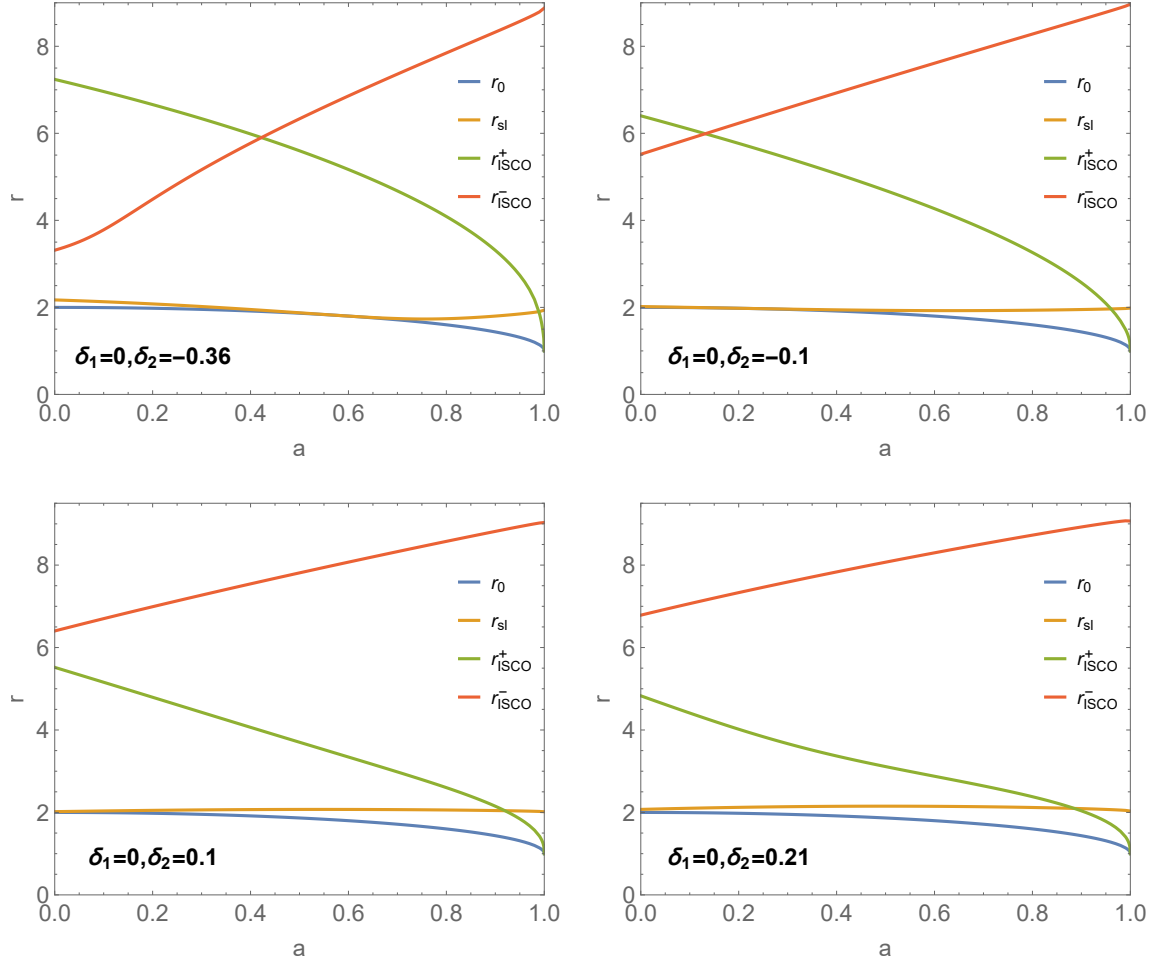


FIG. 3. Radius of innermost stable circular orbit as a function of the spin a . Here we fix $\delta_1 = 0$ and study the influence of δ_2 . r_{ISCO}^+ and r_{ISCO}^- represent the corotating and counter-rotating orbits, respectively. r_0 is the event horizon and r_{sl} is the ergosphere.

We have also checked that the vertically stable condition $\partial_\theta^2 V_{\text{eff}} \leq 0$ is always satisfied for (radially) ISCO in the parameter region (8).

IV. ENERGY EXTRACTION VIA MAGNETIC RECONNECTION

In this section, we investigate the process of harnessing energy from the black hole through magnetic reconnection in the ergoregion, a phenomenon anticipated to be a common occurrence in rapidly spinning black holes. To simplify the analysis, we employ the methodology elucidated in [23] and focus on magnetic reconnection in the surrounding plasma, which rotates around the black hole in a stable circular orbit in the equatorial plane at the Keplerian velocity Ω_K .

To assess the energy density of the outflowing plasma, it is advantageous to evaluate some

quantities in the so-called “zero-angular-momentum-observer” (ZAMO) frame [9]. This is a locally nonrotating frame in which the spacetime is locally Minkowskian

$$ds^2 = -d\hat{t}^2 + \sum_{i=1}^3 (d\hat{x}^i)^2 = \eta_{\mu\nu} d\hat{x}^\mu d\hat{x}^\nu, \quad (24)$$

where the transformation between the ZAMO frame ($\hat{t}, \hat{x}^1 = \hat{r}, \hat{x}^2 = \hat{\theta}, \hat{x}^3 = \hat{\phi}$) and the Boyer-Lindquist coordinates ($t, x^1 = r, x^2 = \theta, x^3 = \phi$) is

$$d\hat{t} = \alpha dt, \quad d\hat{x}^i = \sqrt{g_{ii}} dx^i - \alpha \beta^i dt, \quad (25)$$

with the lapse function α and the shift vector $\beta^i = (0, 0, \beta^\phi)$ being

$$\alpha = \left(-g_{tt} + \frac{g_{t\phi}^2}{g_{\phi\phi}} \right)^{1/2}, \quad \beta^\phi = \frac{\sqrt{g_{\phi\phi}} \omega^\phi}{\alpha}, \quad (26)$$

and $\omega^\phi = -g_{t\phi}/g_{\phi\phi}$ is the angular velocity of the frame dragging. We denote quantities in ZAMO frame with hats. The Keplerian velocity of the corotating bulk plasma in ZAMO becomes

$$\hat{v}_K = \frac{d\hat{x}^\phi}{d\hat{t}} = \frac{\sqrt{g_{\phi\phi}}}{\alpha} \Omega_K - \beta^\phi. \quad (27)$$

Using the one-fluid approximation, the energy-momentum tensor of the plasma can be expressed as

$$T^{\mu\nu} = pg^{\mu\nu} + \omega U^\mu U^\nu + F^\mu{}_\sigma F^{\nu\sigma} - \frac{1}{4} g^{\mu\nu} F^{\rho\sigma} F_{\rho\sigma}, \quad (28)$$

where p, ω, U^μ and $F^{\mu\nu}$ are the proper plasma pressure, enthalpy density, four-velocity, and electromagnetic field tensors, respectively. With the timelike killing vector $\xi = \partial_t$, one can define a covariant conserved energy current $J^\mu \equiv T^{\mu\nu} \xi_\nu$ and the associated energy density $e^\infty \equiv n_\mu J^\mu = -\alpha g_{\mu 0} T^{\mu 0}$, where n^μ is the unit vector normal to timelike hypersurfaces $t = \text{constant}$. At infinity, e^∞ is the energy density measured by static observers, and so is usually called the “energy-at-infinity” density. Assuming a highly efficient conversion of magnetic energy into kinetic energy, so that the electromagnetic component of the energy density can be neglected, and adopting the approximation that the plasma is incompressible and adiabatic, the energy-at-infinity density can be expressed as [23]

$$e^\infty = \alpha \hat{\gamma} \omega (1 + \beta^\phi \hat{v}^\phi) - \frac{\alpha p}{\hat{\gamma}}, \quad (29)$$

where $\hat{\gamma} = \hat{U}^0$ is the Lorentz factor and $\hat{v}^\phi = d\hat{\phi}/d\hat{t}$ is the azimuthal component of the velocity of the outflow plasma. By considering both the accelerated and decelerated parts of the outflowing

plasma, the energy-at-infinity density per enthalpy can ultimately be formulated as [23]

$$\epsilon_{\pm}^{\infty} = \alpha \hat{\gamma}_K \left[(1 + \beta^{\phi} \hat{v}_K)(1 + \sigma_0)^{1/2} \pm \cos \xi (\beta^{\phi} + \hat{v}_K) \sigma_0^{1/2} - \frac{1}{4} \frac{(1 + \sigma_0)^{1/2} \mp \cos \xi \hat{v}_K \sigma_0^{1/2}}{\hat{\gamma}_K^2 (1 + \sigma_0 - \cos^2 \xi \hat{v}_K^2 \sigma_0)} \right], \quad (30)$$

where ξ is the orientation angle between the outflow plasma velocity and the azimuthal direction in the equatorial plane in the local rest frame, $\hat{\gamma}_K = (1 - \hat{v}_K^2)^{-1/2}$ and σ_0 is the plasma magnetization. The signs $+$ and $-$ stand for accelerated and decelerated parts, respectively. From the above equation, it can be seen that the energy-at-infinity density is parametrized by five parameters $\{a, \delta_1, \delta_2, \sigma_0, \xi\}$ as well as the radius $r = r_X$ of the circular orbit of the plasma where the reconnection occurs (X-point).

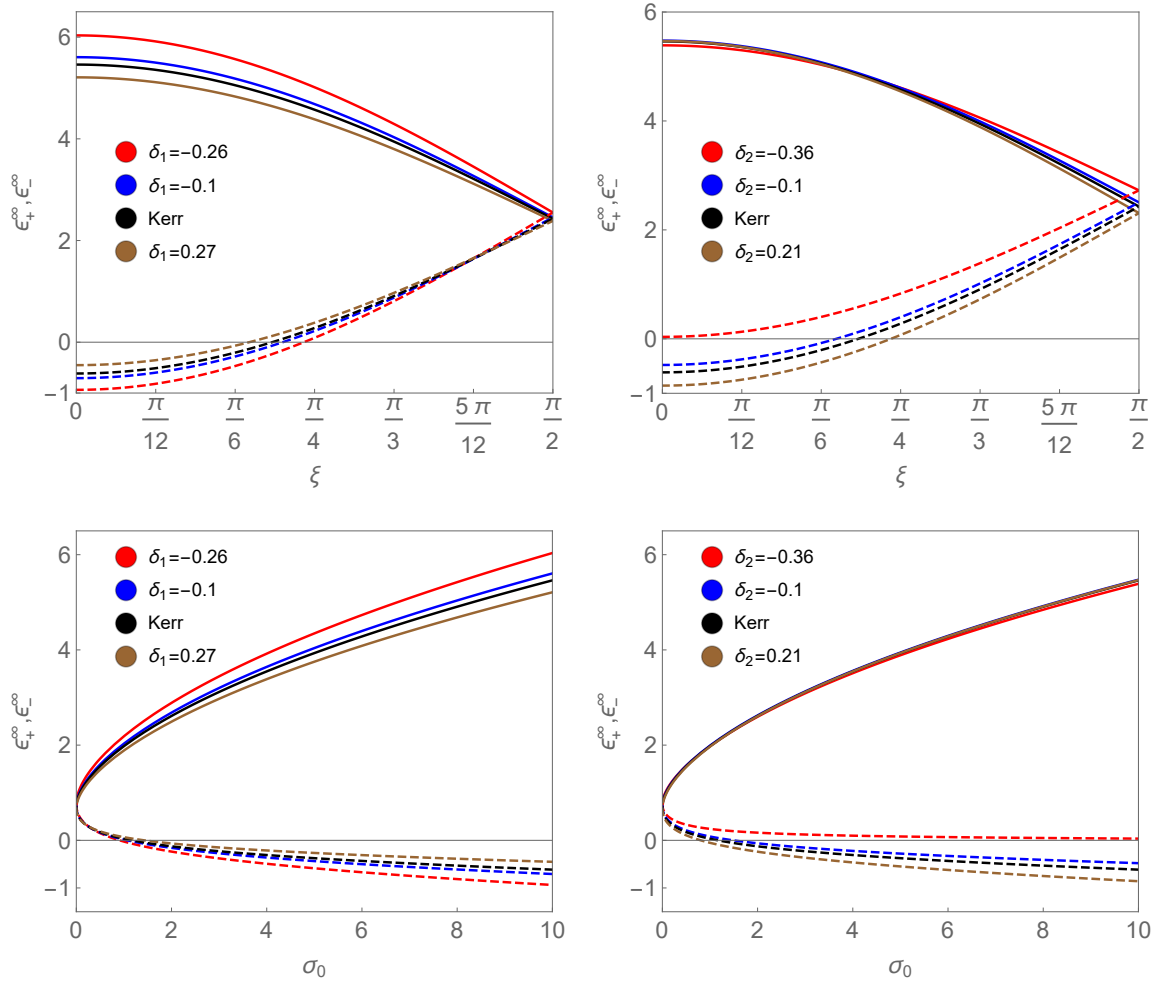


FIG. 4. The energy-at-infinity density ϵ_{\pm}^{∞} as a function of the orientation angle ξ (top panels) and the plasma magnetization σ_0 (bottom panels) for various δ_1 and δ_2 , with $a = 0.99$ and $r_X = r_{\text{ISCO}}^+$. In the top panels, we set $\sigma_0 = 10$, while in the bottom panels, we set $\xi = 0$. In the left panels $\delta_2 = 0$, while in the right panels $\delta_1 = 0$. Solid curves are ϵ_{+}^{∞} while dashed ones are ϵ_{-}^{∞} .

Energy extraction from a black hole involves the requirement that decelerated plasma possesses

negative energy-at-infinity, while accelerated plasma exhibits positive energy-at-infinity exceeding its rest mass and thermal energy, that is

$$\epsilon_-^\infty < 0, \quad \Delta\epsilon_+^\infty = \epsilon_+^\infty - \left(1 - \frac{\Gamma}{\Gamma-1} \frac{p}{\omega}\right) = \epsilon_+^\infty > 0. \quad (31)$$

Here we have assumed the plasma to be relativistically hot with polytropic index $\Gamma = 4/3$.

A. Parameter space analysis

In this subsection, we will perform a parameter space analysis to show the influences of $\{\delta_1, \delta_2\}$ on the permissible regions where the energy extraction conditions (31) are satisfied.

In Fig. 4 we show the effects of $\{\delta_1, \delta_2\}$ on the required orientation angle ξ and the plasma magnetization σ_0 to satisfy the energy extraction conditions (31) for a near-extreme black hole ($a = 0.99$). We take the X-point to be at $r_X = r_{\text{ISCO}}^+$. From the figure we can see that, as in the Kerr case, energy extraction is favored by lower values of ξ but higher values of σ_0 . Moreover, $\epsilon_+^\infty > 0$ is always satisfied, while $\epsilon_-^\infty < 0$ is only satisfied when ξ is less than some upper bound ξ^c and σ_0 exceeds some lower bound σ_0^c . As δ_1 increases from negative to positive values, ξ^c is shifted to smaller values, and σ_0^c is shifted to larger values, while δ_2 has the opposite effect. Furthermore, if δ_2 is negative enough, $\epsilon_-^\infty < 0$ cannot be satisfied for any ξ and σ_0 . Compared to the Kerr case, smaller σ_0^c is required to satisfy the energy extraction conditions when $\delta_2 < 0$ or $\delta_1 > 0$. These results imply that energy extraction is favored by negative δ_1 but positive δ_2 .

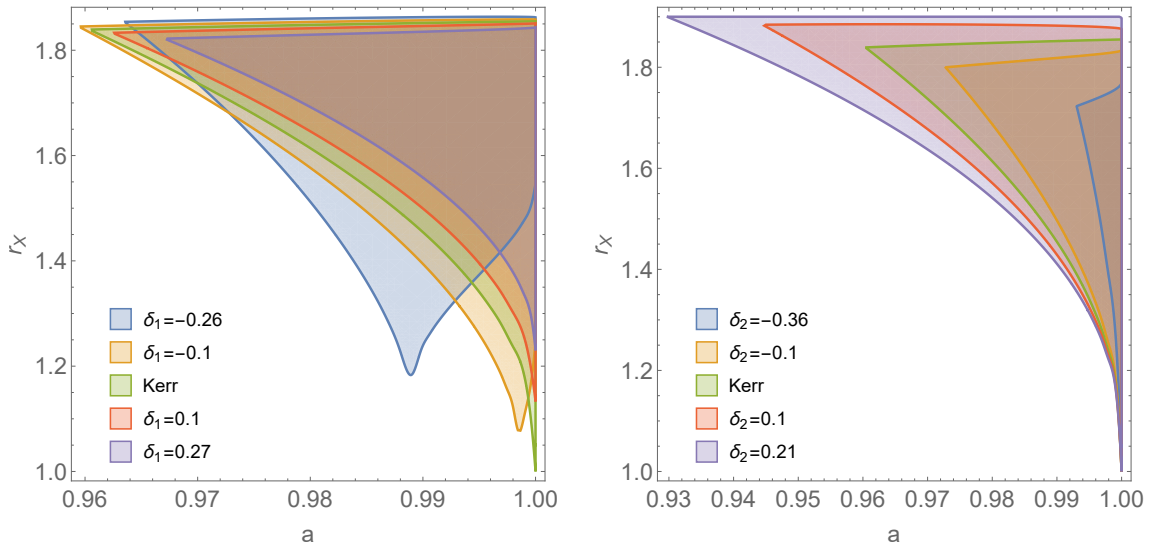


FIG. 5. Permissible regions (shaded) in $a - r_X$ plane where the energy extraction conditions are satisfied for $r_{\text{ISCO}}^+ \leq r_X < r_{\text{sl}}$. We set $\xi = \frac{\pi}{12}$ and $\sigma_0 = 10$. In the left panels $\delta_2 = 0$, while in the right panels $\delta_1 = 0$.

In Fig. 5 we plot the permissible regions in the $a - r_X$ plane where the energy extraction conditions (31) are satisfied for various δ_1 and δ_2 . Note that the bulk plasma is assumed to rotate in a stable circular orbit in the ergoregion, so the permissible regions are additionally constrained by $r_{\text{ISCO}}^+ \leq r_X < r_{\text{sl}}$. Numerically, we found that the lower boundary of the permissible region is given by $r_X = r_{\text{ISCO}}^+$, while the upper boundary is inside the ergosphere. Thus, $r_X < r_{\text{sl}}$ is not sufficient to satisfy the energy extraction conditions. Only when the X-point is deep enough in the ergoregion can the energy extraction conditions be satisfied. From the right panel, it can be seen that as δ_2 decreases from a positive value to a negative value, the permissible region shrinks significantly and a higher a is required to satisfy the energy extraction conditions. It is worth noting that, for $\delta_2 = 0.21$, $a \gtrsim 0.93$ is necessary to fulfill the energy extraction conditions. Conversely, for $\delta_2 = -0.36$, an exceedingly high spin of $a \gtrsim 0.994$ is needed to meet the energy extraction conditions. For comparison, in the Kerr case, $a \gtrsim 0.96$ is necessary to fulfill the energy extraction conditions. This again confirms our previous conclusion that energy extraction is favored by positive δ_2 . However, the influence of δ_1 on the permissible region is not so clear as shown in the left panel. It can be seen that as δ_1 increases from negative to positive, the required lower bound of a first decreases and then increases moderately. This complication is due to the complicated effect of δ_1 on r_{ISCO}^+ as previously shown in Fig. 2.

B. Energy extraction power and efficiency

In this subsection, we analyze the effects of $\{\delta_1, \delta_2\}$ on the power and efficiency of energy extraction.

The power $\mathcal{P}_{\text{extr}}$ per unit enthalpy extracted from the black hole by the escaping plasma can be well-estimated as [23]

$$\mathcal{P}_{\text{extr}} = -\epsilon_-^\infty A_{\text{in}} U_{\text{in}}, \quad (32)$$

where A_{in} is the cross sectional area of the inflowing plasma, which can be estimated as $A_{\text{in}} \sim (r_{\text{sl}}^2 - r_{\text{ISCO}}^2)$ for fast-rotating black holes. The parameter $U_{\text{in}} = \mathcal{O}(10^{-2})$ and $\mathcal{O}(10^{-1})$ for the collisional and collisionless regime respectively.

Figure 6 shows a typical picture of power $\mathcal{P}_{\text{extr}}$ as a function of the X-point location r_X . From the figure it can be seen that, with all other parameters fixed, $\mathcal{P}_{\text{extr}}$ is a monotonically decreasing function of r_X , reaching a maximum at $r_X = r_{\text{ISCO}}^+$. From the left panels, we can see that for fixed r_X the effect of δ_1 on $\mathcal{P}_{\text{extr}}$ is moderate and depends on the spin a . When a is not so extremely

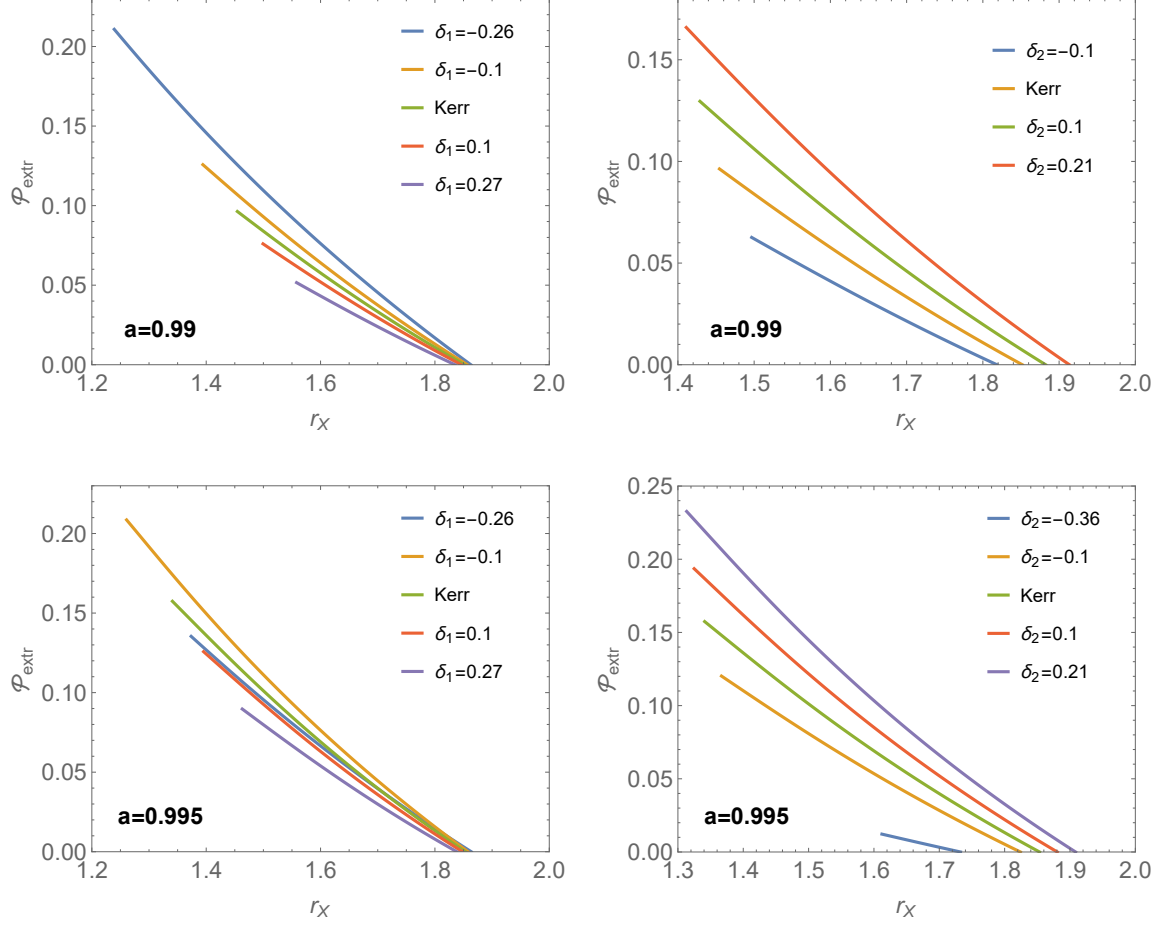


FIG. 6. $\mathcal{P}_{\text{extr}}$ as a function of the X-point location r_X for various $\{\delta_1, \delta_2\}$, with $\xi = \frac{\pi}{12}, \sigma_0 = 10$ and $U_{\text{in}} = 0.1$. r_X is restricted to be in the range $r_{\text{ISCO}}^+ \leq r_X < r_{\text{sl}}$. In the left panels $\delta_2 = 0$, while in the right panels $\delta_1 = 0$.

high, $\mathcal{P}_{\text{extr}}$ is a monotonically decreasing function of δ_1 . However, when a is extremely high, as δ_1 increases, $\mathcal{P}_{\text{extr}}$ first increases and then decreases. From the right panels, we can see that for fixed r_X , $\mathcal{P}_{\text{extr}}$ is a monotonically increasing function of δ_2 . Note that for $a < 0.994$, as we mentioned above, there is no energy extraction for $\delta_2 = -0.36$. For given a , the maximum power for the KRZ black hole can significantly exceed that of the Kerr case when $\{\delta_1, \delta_2\}$ fall within particular ranges. For instance, when $a = 0.99$, $\frac{\mathcal{P}_{\text{extr}}^{\text{max}}(\delta_1 = -0.26, \delta_2 = 0)}{\mathcal{P}_{\text{extr}}^{\text{max}}(\text{Kerr})} \sim 2.0$ and $\frac{\mathcal{P}_{\text{extr}}^{\text{max}}(\delta_1 = 0, \delta_2 = 0.21)}{\mathcal{P}_{\text{extr}}^{\text{max}}(\text{Kerr})} \sim 1.7$. Similarly, for $a = 0.995$, $\frac{\mathcal{P}_{\text{extr}}^{\text{max}}(\delta_1 = -0.1, \delta_2 = 0)}{\mathcal{P}_{\text{extr}}^{\text{max}}(\text{Kerr})} \sim 1.5$ and $\frac{\mathcal{P}_{\text{extr}}^{\text{max}}(\delta_1 = 0, \delta_2 = 0.21)}{\mathcal{P}_{\text{extr}}^{\text{max}}(\text{Kerr})} \sim 1.5$.

To further measure the feasibility of magnetic reconnection energy extraction, it is convenient to define the efficiency of the plasma energization process [23],

$$\eta = \frac{\epsilon_+^{\infty}}{\epsilon_+^{\infty} + \epsilon_-^{\infty}}. \quad (33)$$

If $\eta > 1$, energy is extracted from the black hole. Figure 7 shows a typical picture of the efficiency

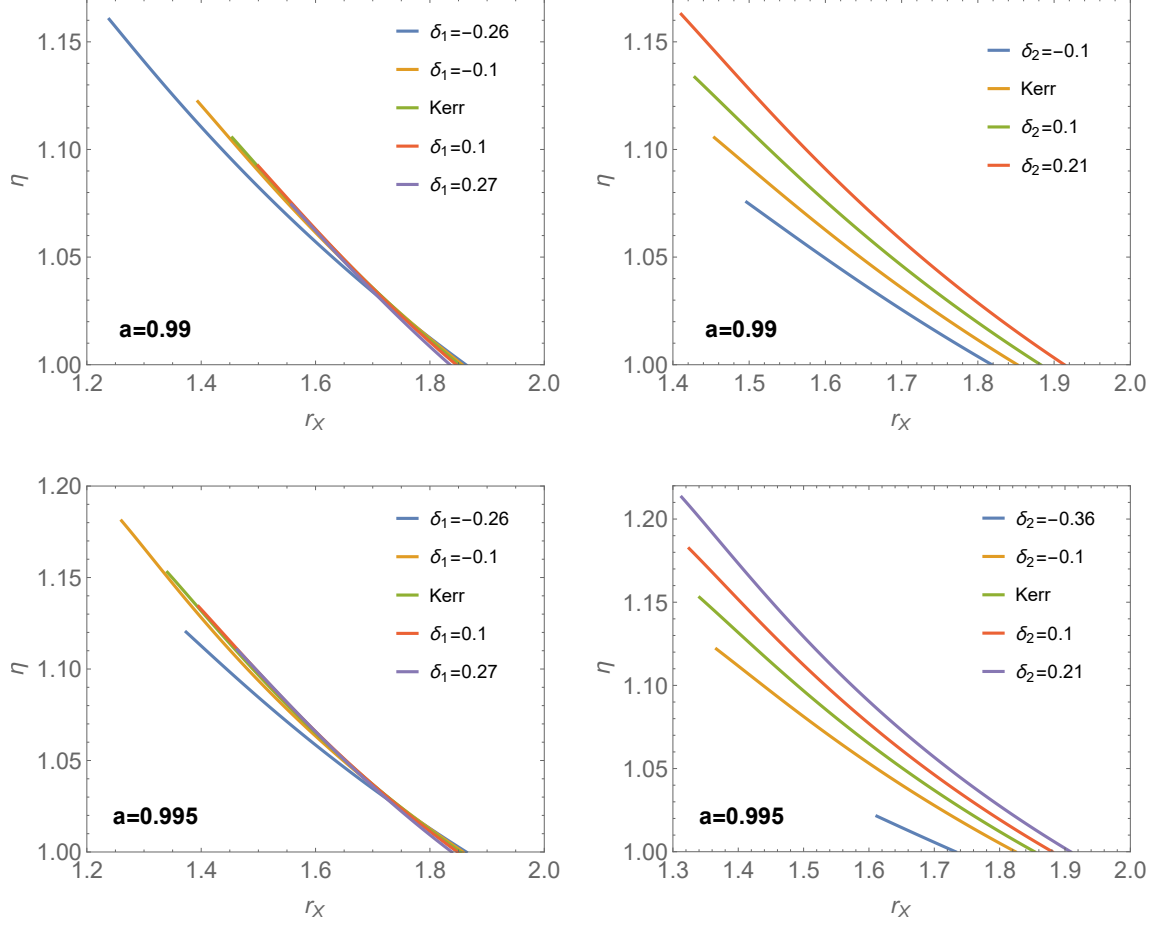


FIG. 7. η as a function of the X-point location r_X for various $\{\delta_1, \delta_2\}$, with $\xi = \frac{\pi}{12}$, $\sigma_0 = 10$ and $U_{\text{in}} = 0.1$. r_X is restricted to be in the range $r_{\text{ISCO}}^+ \leq r_X < r_{\text{sl}}$. In the left panels $\delta_2 = 0$, while in the right panels $\delta_1 = 0$.

η as a function of the X-point location r_X . From the figure it can be seen that, for other fixed parameters, η is a monotonically decreasing function of r_X , reaching a maximum at $r_X = r_{\text{ISCO}}^+$. The right panels show that for fixed r_X , η is a monotonically increasing function of δ_2 . However, the effect of δ_1 on η is complicated and moderately dependent on r_X . When r_X is small, η is a monotonically increasing function of δ_1 . However, if r_X is large enough, η becomes a monotonically decreasing function of δ_1 . For given a , the maximum efficiency for the KRZ black hole can also exceed that of the Kerr case when $\{\delta_1, \delta_2\}$ fall within particular ranges. For instance, when $a = 0.99$, $\frac{\eta^{\text{max}}(\delta_1=-0.26, \delta_2=0)}{\eta^{\text{max}}(\text{Kerr})} \sim 105\%$ and $\frac{\eta^{\text{max}}(\delta_1=0, \delta_2=0.21)}{\eta^{\text{max}}(\text{Kerr})} \sim 106\%$. Similarly, for $a = 0.995$, $\frac{\eta^{\text{max}}(\delta_1=-0.1, \delta_2=0)}{\eta^{\text{max}}(\text{Kerr})} \sim 106\%$ and $\frac{\eta^{\text{max}}(\delta_1=0, \delta_2=0.21)}{\eta^{\text{max}}(\text{Kerr})} \sim 109\%$.

V. SUMMARY AND CONCLUSIONS

In this work, we study energy extraction from the KRZ parametrized black holes via the Comisso-Asenjo mechanism [23], a novel mechanism recently proposed to extract energy from black holes via the magnetic reconnection process. The KRZ metric is a parametrized metric that describes generic stationary and axisymmetric black holes [50], with six parameters introduced to characterize deviations from the Kerr metric. Of these parameters, δ_1 and δ_2 play a crucial role in the physics under consideration, corresponding to deformations of g_{tt} and rotational deformations of the metric, respectively, especially in the near-horizon zone. The values of both parameters are constrained by current astronomical observations (8). We study in detail the ergoregion, the circular geodesics in the equatorial plane, and the energy extraction via magnetic reconnection, and find that these two deformation parameters have significant influences.

Magnetic reconnection takes place in the ergoregion. Following [22], we have assumed that the bulk plasma rotates around the black hole in a circular and stable orbit in the equatorial plane. Such an orbit exists from infinity to ISCO. As shown in Figs. 1, 2 and 3, $\{\delta_1, \delta_2\}$ significantly affects the shape of the ergoregion and the location of ISCO. $\{\delta_1, \delta_2\}$ can enlarge or shrink the ergoregion depending on their signs and the spin a . Specifically, a negative δ_1 and a positive δ_2 promote magnetic reconnection by enlarging the ergoregion. The counter-rotating ISCO r_{ISCO}^- is always outside the ergoregion and is therefore not relevant to the process. The corotating ISCO enters the ergoregion when the spin a is high enough to exceed some critical value a_c . δ_1 has little effect on a_c , while δ_2 has a significant effect on a_c . A higher positive value of δ_2 is advantageous for magnetic reconnection, as it necessitates a lower black hole spin for the process to occur.

To realize energy extraction, the energy extraction conditions (31), $\epsilon_+^\infty > 0$ and $\epsilon_-^\infty < 0$, must be satisfied. We have performed a detailed analysis of the influences of the deformation parameters $\{\delta_1, \delta_2\}$ on the energy extraction conditions in Figs. 4, 5, 6 and 7.

From Fig. 4 it can be seen that an increase in the magnitude of negative δ_1 or positive δ_2 leads to a reduction in the critical plasma magnetization σ_0 required for energy extraction. This observation indicates a preference for energy extraction with negative δ_1 and positive δ_2 . From Fig. 5 it can be seen that as δ_2 decreases from positive to negative, the permissible region in the $a - r_X$ plane to satisfy the energy extraction conditions shrinks significantly and a higher value of a is required. It is noteworthy that if δ_2 is sufficiently negative, an exceedingly high spin (e.g., $a \gtrsim 0.994$ for $\delta_2 = -0.36$) is required to satisfy the energy extraction conditions, posing challenges for energy extraction via this mechanism. This again confirms our previous conclusion that energy

extraction is favored by a large positive δ_2 . This conclusion is further confirmed by examining the effects of the deformation parameters $\{\delta_1, \delta_2\}$ on the power $\mathcal{P}_{\text{extr}}$ (Fig. 6) and efficiency η (Fig. 7). All these results imply that energy extraction is favored by negative δ_1 but positive δ_2 . Compared to the Kerr case, the maximum power and efficiency for the KRZ black hole can be significantly higher.

Typically, the energy of the matter and electromagnetic fields surrounding a black hole is negligible compared to the mass of the black hole. Therefore, in our work, as in the related studies mentioned earlier, we have not considered the backreactions of the surrounding matter and electromagnetic fields on the black hole geometry. Non-Kerr rotating black holes typically have only a small deviation from the Kerr black hole. If the energy of the matter and fields surrounding these black holes is sufficiently high, their backreaction on the geometry can be comparable to the deviation. In this case, it is necessary to consider their effects on the black hole geometry and the energy extraction process. Further studies are needed to fully understand these effects.

ACKNOWLEDGMENTS

This work is supported by the National Natural Science Foundation of China (NNSFC) under Grant No 12075207.

-
- [1] **LIGO Scientific, Virgo** Collaboration, B. P. Abbott *et al.*, “Observation of Gravitational Waves from a Binary Black Hole Merger,” *Phys. Rev. Lett.* **116** no. 6, (2016) 061102, [arXiv:1602.03837 \[gr-qc\]](#).
 - [2] **LIGO Scientific, Virgo** Collaboration, B. P. Abbott *et al.*, “GW151226: Observation of Gravitational Waves from a 22-Solar-Mass Binary Black Hole Coalescence,” *Phys. Rev. Lett.* **116** no. 24, (2016) 241103, [arXiv:1606.04855 \[gr-qc\]](#).
 - [3] **LIGO Scientific, VIRGO** Collaboration, B. P. Abbott *et al.*, “GW170104: Observation of a 50-Solar-Mass Binary Black Hole Coalescence at Redshift 0.2” *Phys. Rev. Lett.* **118** no. 22, (2017) 221101, [arXiv:1706.01812 \[gr-qc\]](#). [Erratum: *Phys.Rev.Lett.* 121, 129901 (2018)].
 - [4] **LIGO Scientific, Virgo** Collaboration, B. P. Abbott *et al.*, “GW170814: A Three-Detector Observation of Gravitational Waves from a Binary Black Hole Coalescence,” *Phys. Rev. Lett.* **119** no. 14, (2017) 141101, [arXiv:1709.09660 \[gr-qc\]](#).
 - [5] **LIGO Scientific, Virgo** Collaboration, R. Abbott *et al.*, “GW190521: A Binary Black Hole Merger with a Total Mass of $150M_{\odot}$,” *Phys. Rev. Lett.* **125** no. 10, (2020) 101102, [arXiv:2009.01075 \[gr-qc\]](#).

- [6] **Event Horizon Telescope** Collaboration, K. Akiyama *et al.*, “First M87 Event Horizon Telescope Results. I. The Shadow of the Supermassive Black Hole,” *Astrophys. J. Lett.* **875** (2019) L1, [arXiv:1906.11238 \[astro-ph.GA\]](#).
- [7] D. Christodoulou, “Reversible and irreversible transformations in black hole physics,” *Phys. Rev. Lett.* **25** (1970) 1596–1597.
- [8] R. Penrose, “Gravitational collapse: The role of general relativity,” *Riv. Nuovo Cim.* **1** (1969) 252–276.
- [9] J. M. Bardeen, W. H. Press, and S. A. Teukolsky, “Rotating black holes: Locally nonrotating frames, energy extraction, and scalar synchrotron radiation,” *Astrophys. J.* **178** (1972) 347.
- [10] R. M. Wald, “Energy Limits on the Penrose Process,” *Astrophys. J.* **191** (1974) 231.
- [11] S. A. Teukolsky and W. H. Press, “Perturbations of a rotating black hole. III - Interaction of the hole with gravitational and electromagnetic radiation,” *Astrophys. J.* **193** (1974) 443–461.
- [12] T. Piran, J. Shaham, and J. Katz, “High efficiency of the penrose mechanism for particle collisions,” *Astrophys. J. Lett.* **196** (1975) L107.
- [13] R. D. Blandford and R. L. Znajek, “Electromagnetic extractions of energy from Kerr black holes,” *Mon. Not. Roy. Astron. Soc.* **179** (1977) 433–456.
- [14] M. Takahashi, S. Nitta, Y. Tatematsu, and A. Tomimatsu, “Magnetohydrodynamic Flows in Kerr Geometry: Energy Extraction from Black Holes,” *Astrophys. J.* **363** (Nov., 1990) 206.
- [15] H. K. Lee, R. A. M. J. Wijers, and G. E. Brown, “The Blandford-Znajek process as a central engine for a gamma-ray burst,” *Phys. Rept.* **325** (2000) 83–114, [arXiv:astro-ph/9906213](#).
- [16] A. Tchekhovskoy, J. C. McKinney, and R. Narayan, “Simulations of Ultrarelativistic Magnetodynamic Jets from Gamma-ray Burst Engines,” *Mon. Not. Roy. Astron. Soc.* **388** (2008) 551, [arXiv:0803.3807 \[astro-ph\]](#).
- [17] S. S. Komissarov and M. V. Barkov, “Activation of the Blandford-Znajek mechanism in collapsing stars,” *Mon. Not. Roy. Astron. Soc.* **397** (2009) 1153, [arXiv:0902.2881 \[astro-ph.HE\]](#).
- [18] J. C. McKinney and C. F. Gammie, “A Measurement of the electromagnetic luminosity of a Kerr black hole,” *Astrophys. J.* **611** (2004) 977–995, [arXiv:astro-ph/0404512](#).
- [19] J. F. Hawley and J. H. Krolik, “Magnetically driven jets in the kerr metric,” *Astrophys. J.* **641** (2006) 103–116, [arXiv:astro-ph/0512227](#).
- [20] S. S. Komissarov and J. C. McKinney, “Meissner effect and Blandford-Znajek mechanism in conductive black hole magnetospheres,” *Mon. Not. Roy. Astron. Soc.* **377** (2007) L49–L53, [arXiv:astro-ph/0702269](#).
- [21] A. Tchekhovskoy, R. Narayan, and J. C. McKinney, “Efficient Generation of Jets from Magnetically Arrested Accretion on a Rapidly Spinning Black Hole,” *Mon. Not. Roy. Astron. Soc.* **418** (2011) L79–L83, [arXiv:1108.0412 \[astro-ph.HE\]](#).
- [22] S. Koide and K. Arai, “Energy extraction from a rotating black hole by magnetic reconnection in ergosphere,” *Astrophys. J.* **682** (2008) 1124, [arxiv:0805.0044 \[astro-ph\]](#).

- [23] L. Comisso and F. A. Asenjo, “Magnetic reconnection as a mechanism for energy extraction from rotating black holes,” *Phys. Rev. D* **103** no. 2, (2021) 023014, [arxiv:2012.00879 \[astro-ph.HE\]](#).
- [24] K. Parfrey, A. Philippov, and B. Cerutti, “First-Principles Plasma Simulations of Black-Hole Jet Launching,” *Phys. Rev. Lett.* **122** no. 3, (2019) 035101, [arXiv:1810.03613 \[astro-ph.HE\]](#).
- [25] S. S. Komissarov, “Observations of the Blandford-Znajek and the MHD Penrose processes in computer simulations of black hole magnetospheres,” *Mon. Not. Roy. Astron. Soc.* **359** (2005) 801–808, [arXiv:astro-ph/0501599](#).
- [26] W. E. East and H. Yang, “Magnetosphere of a spinning black hole and the role of the current sheet,” *Phys. Rev. D* **98** no. 2, (2018) 023008, [arXiv:1805.05952 \[astro-ph.HE\]](#).
- [27] B. Ripperda, F. Bacchini, and A. Philippov, “Magnetic Reconnection and Hot Spot Formation in Black Hole Accretion Disks,” *Astrophys. J.* **900** no. 2, (2020) 100, [arXiv:2003.04330 \[astro-ph.HE\]](#).
- [28] L. Comisso, M. Lingam, Y.-M. Huang, and A. Bhattacharjee, “General theory of the plasmoid instability,” *Physics of Plasmas* **23** no. 10, (2016) 100702, [arxiv:1608.04692 \[astro-ph, physics:math-ph, physics:physics\]](#).
- [29] D. A. Uzdensky, N. F. Loureiro, and A. A. Schekochihin, “Fast magnetic reconnection in the plasmoid-dominated regime,” *Phys. Rev. Lett.* **105** (2010) 235002, [arxiv:1008.3330 \[astro-ph.SR\]](#).
- [30] L. Comisso, M. Lingam, Y.-M. Huang, and A. Bhattacharjee, “Plasmoid instability in forming current sheets,” *Astrophys. J.* **850** no. 2, (2017) 142, [arxiv:1707.01862 \[astro-ph.HE\]](#).
- [31] W. Daughton, V. Roytershteyn, B. J. Albright, H. Karimabadi, L. Yin, and K. J. Bowers, “Transition from collisional to kinetic regimes in large-scale reconnection layers,” *Phys. Rev. Lett.* **103** no. 6, (2009) 065004.
- [32] A. Bhattacharjee, Y.-M. Huang, H. Yang, and B. Rogers, “Fast reconnection in high-lundquist-number plasmas due to secondary tearing instabilities,” *Physics of Plasmas* **16** no. 11, (2009) 112102, [arxiv:0906.5599 \[physics\]](#).
- [33] K. Mori *et al.*, “NuSTAR discovery of a 3.76-second transient magnetar near Sagittarius A*,” *Astrophys. J. Lett.* **770** (2013) L23, [arXiv:1305.1945 \[astro-ph.HE\]](#).
- [34] J. A. Kennea *et al.*, “Swift Discovery of a New Soft Gamma Repeater, SGR J1745-29, near Sagittarius A*,” *Astrophys. J. Lett.* **770** (2013) L24, [arXiv:1305.2128 \[astro-ph.HE\]](#).
- [35] R. P. Eatough *et al.*, “A strong magnetic field around the supermassive black hole at the centre of the Galaxy,” *Nature* **501** (2013) 391–394, [arXiv:1308.3147 \[astro-ph.GA\]](#).
- [36] S. A. Olausen and V. M. Kaspi, “The McGill Magnetar Catalog,” *Astrophys. J. Suppl.* **212** (2014) 6, [arXiv:1309.4167 \[astro-ph.HE\]](#).
- [37] **Event Horizon Telescope** Collaboration, K. Akiyama *et al.*, “First M87 Event Horizon Telescope Results. VIII. Magnetic Field Structure near The Event Horizon,” *Astrophys. J. Lett.* **910** no. 1, (2021) L13, [arXiv:2105.01173 \[astro-ph.HE\]](#).
- [38] P. Kanti, N. E. Mavromatos, J. Rizos, K. Tamvakis, and E. Winstanley, “Dilatonic black holes in

- higher curvature string gravity,” *Phys. Rev. D* **54** (1996) 5049–5058, [arXiv:hep-th/9511071](#).
- [39] D. Ayzenberg and N. Yunes, “Slowly-Rotating Black Holes in Einstein-Dilaton-Gauss-Bonnet Gravity: Quadratic Order in Spin Solutions,” *Phys. Rev. D* **90** (2014) 044066, [arXiv:1405.2133 \[gr-qc\]](#). [Erratum: *Phys.Rev.D* 91, 069905 (2015)].
- [40] A. Maselli, P. Pani, L. Gualtieri, and V. Ferrari, “Rotating black holes in Einstein-Dilaton-Gauss-Bonnet gravity with finite coupling,” *Phys. Rev. D* **92** no. 8, (2015) 083014, [arXiv:1507.00680 \[gr-qc\]](#).
- [41] B. Kleihaus, J. Kunz, S. Mojica, and E. Radu, “Spinning black holes in Einstein–Gauss-Bonnet–dilaton theory: Nonperturbative solutions,” *Phys. Rev. D* **93** no. 4, (2016) 044047, [arXiv:1511.05513 \[gr-qc\]](#).
- [42] K. D. Kokkotas, R. A. Konoplya, and A. Zhidenko, “Analytical approximation for the Einstein-dilaton-Gauss-Bonnet black hole metric,” *Phys. Rev. D* **96** no. 6, (2017) 064004, [arXiv:1706.07460 \[gr-qc\]](#).
- [43] N. Yunes and F. Pretorius, “Dynamical Chern-Simons Modified Gravity. I. Spinning Black Holes in the Slow-Rotation Approximation,” *Phys. Rev. D* **79** (2009) 084043, [arXiv:0902.4669 \[gr-qc\]](#).
- [44] K. Yagi, N. Yunes, and T. Tanaka, “Slowly Rotating Black Holes in Dynamical Chern-Simons Gravity: Deformation Quadratic in the Spin,” *Phys. Rev. D* **86** (2012) 044037, [arXiv:1206.6130 \[gr-qc\]](#). [Erratum: *Phys.Rev.D* 89, 049902 (2014)].
- [45] R. McNees, L. C. Stein, and N. Yunes, “Extremal black holes in dynamical Chern–Simons gravity,” *Class. Quant. Grav.* **33** no. 23, (2016) 235013, [arXiv:1512.05453 \[gr-qc\]](#).
- [46] T. Delsate, C. Herdeiro, and E. Radu, “Non-perturbative spinning black holes in dynamical Chern–Simons gravity,” *Phys. Lett. B* **787** (2018) 8–15, [arXiv:1806.06700 \[gr-qc\]](#).
- [47] A. Sen, “Rotating charged black hole solution in heterotic string theory,” *Phys. Rev. Lett.* **69** (1992) 1006–1009, [arXiv:hep-th/9204046](#).
- [48] S. Vigeland, N. Yunes, and L. Stein, “Bumpy Black Holes in Alternate Theories of Gravity,” *Phys. Rev. D* **83** (2011) 104027, [arXiv:1102.3706 \[gr-qc\]](#).
- [49] T. Johannsen, “Regular Black Hole Metric with Three Constants of Motion,” *Phys. Rev. D* **88** no. 4, (2013) 044002, [arXiv:1501.02809 \[gr-qc\]](#).
- [50] R. Konoplya, L. Rezzolla, and A. Zhidenko, “General parametrization of axisymmetric black holes in metric theories of gravity,” *Phys. Rev. D* **93** no. 6, (2016) 064015, [arxiv:1602.02378 \[gr-qc\]](#).
- [51] G. O. Papadopoulos and K. D. Kokkotas, “Preserving Kerr symmetries in deformed spacetimes,” *Class. Quant. Grav.* **35** no. 18, (2018) 185014, [arXiv:1807.08594 \[gr-qc\]](#).
- [52] Z. Carson and K. Yagi, “Asymptotically flat, parameterized black hole metric preserving Kerr symmetries,” *Phys. Rev. D* **101** no. 8, (2020) 084030, [arXiv:2002.01028 \[gr-qc\]](#).
- [53] S.-W. Wei, H.-M. Wang, Y.-P. Zhang, and Y.-X. Liu, “Effects of tidal charge on magnetic reconnection and energy extraction from spinning braneworld black hole,” *JCAP* **04** no. 04, (2022) 050, [arxiv:2201.12729 \[gr-qc\]](#).

- [54] W. Liu, “Energy extraction via magnetic reconnection in the ergosphere of a rotating non-kerr black hole,” *Astrophys. J.* **925** no. 2, (2022) 149, [arxiv:2204.07338 \[astro-ph.HE\]](#).
- [55] A. Carleo, G. Lambiase, and L. Mastrototaro, “Energy extraction via magnetic reconnection in lorentz breaking kerr–sen and kiselev black holes,” *Eur. Phys. J. C* **82** no. 9, (2022) 776, [arxiv:2206.12988 \[gr-qc\]](#).
- [56] M. Khodadi, “Magnetic reconnection and energy extraction from a spinning black hole with broken lorentz symmetry,” *Phys. Rev. D* **105** no. 2, (2022) 023025, [arxiv:2201.02765 \[gr-qc\]](#).
- [57] Z. Li, X.-K. Guo, and F. Yuan, “Energy extraction from rotating regular black hole via comisso-asenjo mechanism,” *Phys. Rev. D* **108** no. 4, (2023) 044067, [arxiv:2304.08831 \[gr-qc\]](#).
- [58] Z. Li and F. Yuan, “Energy extraction via comisso-asenjo mechanism from rotating hairy black hole,” *Phys. Rev. D* **108** no. 2, (2023) 024039, [arxiv:2304.12553 \[gr-qc\]](#).
- [59] M. Khodadi, D. F. Mota, and A. Sheykhi, “Harvesting energy driven by comisso-asenjo process from kerr-mog black holes,” *JCAP* **10** (2023) 034, [arxiv:2307.00478 \[astro-ph.HE\]](#).
- [60] S. Shaymatov, M. Alloqulov, B. Ahmedov, and A. Wang, “A kerr-newman-mog black hole’s impact on the magnetic reconnection,” *arXiv:2307.03012 [gr-qc]* (2023) , [arxiv:2307.03012 \[gr-qc\]](#).
- [61] C.-H. Wang, C.-Q. Pang, and S.-W. Wei, “Extracting energy via magnetic reconnection from kerr–de sitter black holes,” *Phys. Rev. D* **106** no. 12, (2022) 124050, [arxiv:2209.08837 \[gr-qc\]](#).
- [62] Y. Ni, J. Jiang, and C. Bambi, “Testing the kerr metric with the iron line and the krz parametrization,” *JCAP* **09** no. 09, (2016) 014, [arxiv:1607.04893 \[gr-qc\]](#).
- [63] S. Nampalliwar, S. Xin, S. Srivastava, A. B. Abdikamalov, D. Ayzenberg, C. Bambi, T. Dauser, J. A. Garcia, and A. Tripathi, “Testing general relativity with x-ray reflection spectroscopy: The konoplya-rezzolla-zhidenko parametrization,” *Phys. Rev. D* **102** no. 12, (2020) 124071, [arxiv:1903.12119 \[gr-qc\]](#).
- [64] S. Li and W.-B. Han, “A full waveform model for arbitrarily axis-symmetric black hole mergers,” *Phys. Rev. D* **108** no. 8, (2023) 083032, [arxiv:2307.00797 \[gr-qc\]](#).
- [65] A. B. Abdikamalov, D. Ayzenberg, C. Bambi, S. Nampalliwar, and A. Tripathi, “Constraining the krz deformation parameters i: Limits from supermassive black hole x-ray data,” *Phys. Rev. D* **104** no. 2, (2021) 024058, [arxiv:2104.04183 \[astro-ph.HE\]](#).
- [66] R. A. Konoplya, J. Kunz, and A. Zhidenko, “Blandford-Znajek mechanism in the general stationary axially-symmetric black-hole spacetime,” *JCAP* **12** no. 12, (2021) 002, [arXiv:2102.10649 \[gr-qc\]](#).
- [67] S. Shaymatov, B. Ahmedov, M. De Laurentis, M. Jamil, Q. Wu, A. Wang, and M. Azreg-Aïnou, “On the Parameters of the Spherically Symmetric Parameterized Rezzolla–Zhidenko Spacetime through Solar System Tests, the Orbit of the S2 Star about Sgr A*, and Quasiperiodic Oscillations,” *Astrophys. J.* **959** no. 1, (2023) 6, [arXiv:2307.10804 \[gr-qc\]](#).